

Modeling of unreinforced brick walls under in-plane shear & compression loading

Arsalan Kalali^a and Mohammad Zaman Kabir*

Department of Civil Engineering, Amirkabir University of Technology (Tehran Polytechnic), Tehran, Iran

(Received June 23, 2009, Accepted June 16, 2010)

Abstract. The study of the seismic vulnerability of masonry buildings requires structural properties of walls such as stiffness, ultimate load capacity, etc. In this article, a method is suggested for modeling the masonry walls under in-plane loading. At the outset, a set of analytical equations was established for determining the elastic properties of an equivalent homogeneous material of masonry. The results for homogenized unreinforced brick walls through detailed modeling were compared in different manners such as solid and perforated walls, in-plane and out-of-plane loading, etc, and it was found that this method provides suitable accuracy in estimation of the wall linear properties. Furthermore, comparison of the results of proposed modeling with experimental out coming indicated that this model considers the non linear properties of the wall such as failure pattern, performance curve and ultimate strength, and would be appropriate to establish a parametric study on those prone factors. The proposed model is complicated; therefore, efforts need to be made in order to overcome the convergency problems which will be included in this study. The nonlinear model is basically semi-macro but through a series of actions, it can be simplified to a macro model.

Keywords: unreinforced brick walls; micro modeling; macro modeling; homogenization; analysis; stiffness; strength; failure pattern.

1. Introduction

Existing unreinforced masonry buildings constitute a significant part of buildings throughout the world. Recent earthquakes have proved the seismic vulnerability of these buildings since a large number of these types of constructions are located in the seismic prone regions without adequate strength and capacity against earthquake loading. Thus, the seismic vulnerability assessment of these structures is an important need and improvement in their performance is of paramount important. In order to overcome to this issue, the assessment methods and strengthening techniques are being developed regularly, (Benedetti and Steli 2008, Roca 2006, Shrive 2006).

Unreinforced masonry shear walls are often used as the main structural components of masonry buildings responsible for carrying the lateral loading such as wind and earthquake loads. The lateral and vertical loads lead to tension and shear combined with compression within the masonry walls. These walls have large in-plane stiffness and strength. In view of the significance of in-plane

*Corresponding author, Associate Professor, E-mail: mzkabir@aut.ac.ir

^aPh.D. Candidate

performance of these walls, the focal point of this research was conducted in this direction.

For analyzing the brick structures, different researchers have chosen one of the following methods (Chaimoon and Attard 2007, Gabor *et al.* 2006a, b):

1. Micro modeling; masonry material is considered as a composite material where components (brick and mortar) are modeled separately. This modeling method is difficult and time consuming and needs numerous input data such as mechanical properties of brick and mortar, geometrical properties of bricks and bed and head joints of mortar, style and pattern of arrangement of bricks, etc.

2. Macro modeling; masonry material is considered as a homogeneous material where the mechanical properties are different from its components (brick and mortar) and masonry components are smeared into an averaged continuum. This equivalent homogeneous material can be considered as isotropic, orthotropic, etc. This method is simple and quick and would require very little input data.

For analysis and seismic vulnerability assessment of masonry buildings, making use of micro modeling is very complicated and rather impractical due to the pattern of arrangement of bricks and bed and head joints of mortar and their large quantity. On the other hand, for performing macro modeling, the properties of equivalent homogeneous material must be determined; therefore different methods for homogenization of unreinforced brick walls and macro modeling have been presented. In the existing analytical equations, with regard to determining the elastic properties of equivalent homogeneous material of masonry, only bricks and bed joints of mortar were taken into consideration for simplicity and reducing the effect of head joints of mortar, (Chaimoon and Attard 2007, Gabor *et al.* 2006a, b). For this reason and to develop and improve of existing analytical equations, the effect of head joints of mortar is also taken into account.

With regard to the style of arrangement of bricks and bed and head joints of mortar in a brick wall which makes the wall stiffness in different directions dissimilar; the equivalent homogenous material of masonry is considered as orthotropic and also nine independent parameters needed for defining it, were established. Subsequently, the results of these hypotheses and equations are compared with micro modeling. The resultant simplicity of the suggested equations is significant, so that for modeling of an unreinforced brick wall, without paying any attention to the style of arrangement of bricks and bed and head mortar joints, the only requisite is to draw a rectangular block, assign mechanical properties of the equivalent homogenous material, mesh the model and then define the boundary conditions and apply the loading.

Thereafter, in order to study the diagonal fracture of walls, the diagonal compression test of masonry panels is modeled and the effects of different parameters are evaluated.

Afterwards, for investigating the nonlinear behavior of unreinforced brick walls under shear and compression, a finite element model is suggested. In this model, nonlinear continuum elements are used for simulation of cracking and crushing of bricks, moreover contact elements are placed for considering the sliding, opening and closing of joints. Then, some comparisons with experimental results are also carried out.

2. Establishment of elastic constants of equivalent homogenous material of masonry

In this section, σ , ε , E , τ , γ , G , P , V , δ and Δ denote the normal stress, normal strain, modulus of elasticity, shear stress, shear strain, shear modulus, axial force, shear force and deformations,

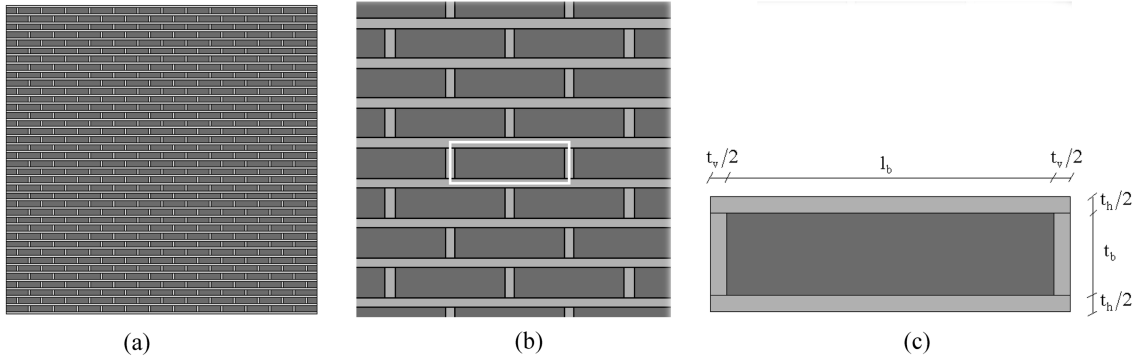


Fig. 1 The unreinforced brick wall and its constituent element

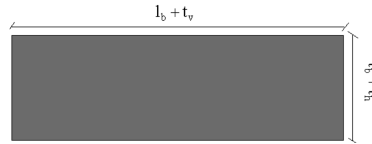


Fig. 2 The generated element by the process of homogenization

respectively. Also, subscripts ‘*b*’, ‘*m*’, ‘*h*’, ‘*v*’, ‘*w*’ and ‘*p*’ were used in the following equations refer to the brick, mortar, bed joint of mortar, head joint of mortar, brick wall and equivalent homogeneous material of masonry, respectively.

As shown in Fig. 1(a), in unreinforced brick walls, the constituent element is shown in Figs. 1(b) and 1(c) that makes up the wall with its replication.

The objective is specifying the mechanical properties of orthotropic homogeneous material equal to the element shown in Fig. 1(c) which is illustrated in Fig. 2.

2.1 Determination of elastic modulus

For calculating E_p^y (modulus of elasticity of orthotropic homogenous material in *y* direction), the following steps have been undertaken.

According to the compatibility of deformations in Figs. 3(a) and 3(b), it is concluded that

$$\delta_e^y = \delta_b^y = \delta_v^y \quad \Rightarrow \quad \varepsilon_e^y t_b = \varepsilon_b^y t_b = \varepsilon_v^y t_b$$

$$\Rightarrow \begin{cases} \sigma_b^y = (E_b/E_e^y) \sigma_y \\ \sigma_v^y = (E_m/E_e^y) \sigma_y \end{cases} \quad (1)$$

The letter *e* is referred to the homogenous material equal to brick and head joints of mortar. According to the equilibrium of forces in Figs. 3(a) and 3(b), results in

$$P_e^y = P_b^y + P_v^y$$

$$\sigma_y (l_b + t_v) t_w = \sigma_b^y l_b t_w + \sigma_v^y t_v t_w \quad (2)$$

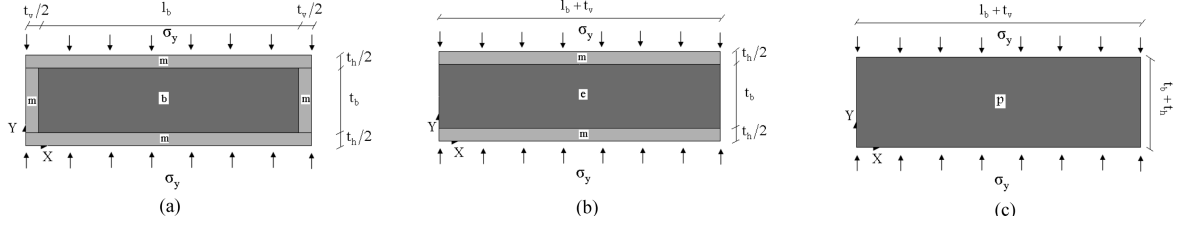


Fig. 3 Steps in the process of homogenization

The combination of Eqs. (1) and (2) yields

$$E_e^y = (E_b l_b + E_m t_v) / (l_b + t_v) \quad (3)$$

Based on the equilibrium of forces in Figs. 3(b) and 3(c), as

$$P_p^y = P_e^y = P_h^y \quad \Rightarrow \quad \sigma_y (l_b + t_v) t_w = \sigma_e^y (l_b + t_v) t_w = \sigma_h^y (l_b + t_v) t_w$$

$$\begin{cases} \varepsilon_e^y = (E_p^y / E_e^y) \varepsilon_p^y \\ \varepsilon_h^y = (E_p^y / E_m) \varepsilon_p^y \end{cases} \quad (4)$$

Considering the compatibility of deformations in Figs. 3(b) and 3(c), leads to

$$\delta_p^y = \delta_e^y + \delta_h^y$$

$$\Rightarrow \varepsilon_p^y (t_b + t_h) = \varepsilon_e^y t_b + \varepsilon_h^y t_h \quad (5)$$

As a result of combining Eqs. (4) and (5), the equivalent modulus of elasticity in y direction becomes

$$E_p^y = (E_e^y E_m (t_b + t_h)) / (E_e^y t_h + E_m t_b) \quad (6)$$

And, finally, by substituting for E_e^y in Eq. (6), results in

$$E_p^y = \frac{E_m (E_b l_b + E_m t_v) (t_b + t_h)}{E_b l_b t_h + E_m (l_b t_b + t_b t_v + t_h t_v)} \quad (7)$$

2.2 Determination of shear modulus

For calculating G_p^{xy} (shear modulus of orthotropic homogenous material in x - y plane), the deformations in x and y directions are taken into consideration. By considering the deformation in x direction as shown in Fig. 4 and according to the compatibility of deformations in Figs. 4(a) and 4(b), it is concluded that

$$\Delta_e^x = \Delta_b^x = \Delta_v^x \quad \Rightarrow \quad \gamma_e^{xy1} t_b = \gamma_b^{xy1} t_b = \gamma_v^{xy1} t_b$$

$$\Rightarrow \begin{cases} \tau_b^{yx} = (G_b / G_e^{xy1}) \tau_e^{yx} \\ \tau_v^{yx} = (G_m / G_e^{xy1}) \tau_e^{yx} \end{cases} \quad (8)$$

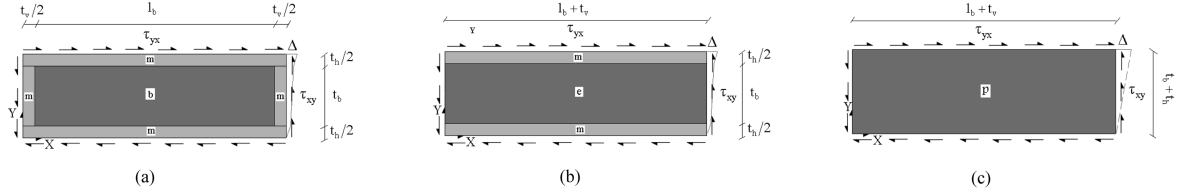


Fig. 4 Steps in the process of homogenization

Based on the equilibrium of forces in Figs. 4(a) and 4(b), leads to

$$\begin{aligned} V_e^x &= V_b^x + V_v^x \\ \Rightarrow \tau_e^{yx} (l_b + t_v) t_w &= \tau_b^{yx} l_b t_w + \tau_v^{yx} t_v t_w \end{aligned} \quad (9)$$

Combining Eqs. (8) and (9), one can obtain

$$G_e^{xy1} = (G_b l_b + G_m t_v) / (l_b + t_v) \quad (10)$$

According to the equilibrium of forces in Figs. 4(b) and 4(c), results in

$$\begin{aligned} V_p^x = V_e^x = V_h^x &\quad \Rightarrow \tau_{yx} (l_b + t_v) t_w = \tau_e^{yx} (l_b + t_v) t_w = \tau_h^{yx} (l_b + t_v) t_w \\ \Rightarrow \begin{cases} \gamma_e^{xy1} = (G_p^{xy1} / G_e^{xy1}) \gamma_p^{xy1} \\ \gamma_h^{xy1} = (G_p^{xy1} / G_m) \gamma_p^{xy1} \end{cases} \end{aligned} \quad (11)$$

Based on the compatibility of deformations in Figs. 4(b) and 4(c), it is concluded that

$$\begin{aligned} \Delta_p^x &= \Delta_e^x + \Delta_h^x \\ \Rightarrow \gamma_p^{xy1} (t_b + t_h) &= \gamma_e^{xy1} t_b + \gamma_h^{xy1} t_h \end{aligned} \quad (12)$$

By combining Eqs. (11) and (12), one gets

$$G_p^{xy1} = (G_e^{xy1} G_m (t_b + t_h)) / (G_e^{xy1} t_h + G_m t_b) \quad (13)$$

By substituting for G_e^{xy1} in Eq. (13)

$$G_p^{xy1} = \frac{G_m (G_b l_b + G_m t_v) (t_b + t_h)}{G_b l_b t_h + G_m (l_b t_b + t_b t_v + t_h t_v)} \quad (14)$$

Considering the deformation in y direction as shown in Fig. 5 and similarly, results in

$$G_p^{xy2} = \frac{G_m [G_b (l_b t_b + t_b t_v + t_h t_v) + G_m l_b t_h]}{(G_b t_v + G_m l_b) (t_b + t_h)} \quad (15)$$

According to Fig. 6

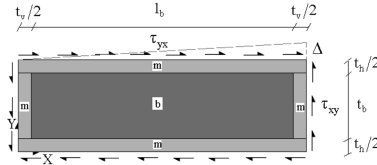


Fig. 5 Determination of G_p^{xy2}

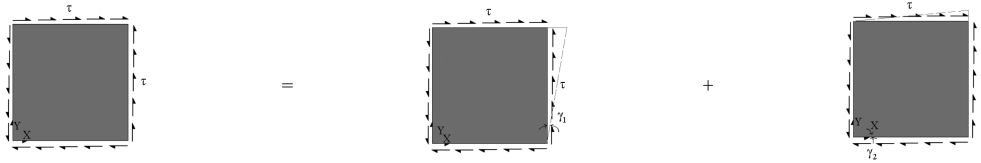


Fig. 6 Superposition in shear deformations

$$\begin{aligned} \gamma_p &= \gamma_p^1/2 + \gamma_p^2/2 \quad \Rightarrow \tau/G_p = \tau/(2G_p^1) + \tau/(2G_p^2) \\ \Rightarrow G_p &= 2G_p^1 G_p^2 / (G_p^1 + G_p^2) \end{aligned} \tag{16}$$

Based on Eqs. (14), (15) and (16), the following relation can be written

$$G_p^{xy} = 2G_p^{xy1} G_p^{xy2} / (G_p^{xy1} + G_p^{xy2}) \tag{17}$$

2.3 Determination of Poisson's ratios

For calculating ν_p^{xy} and ν_p^{yx} (Poisson's ratios of orthotropic homogenous material in x - y plane), the steps as shown in Fig. 7 are followed.

For determining ν_e^{xy} , Fig. 8 is considered.

According to the compatibility of deformations in Figs. 8(a) and 8(b), it is concluded that

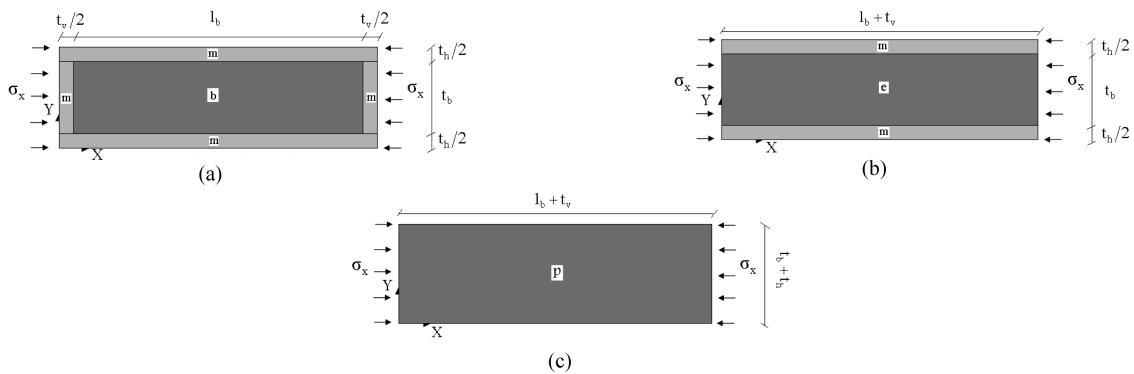


Fig. 7 Steps in the process of homogenization

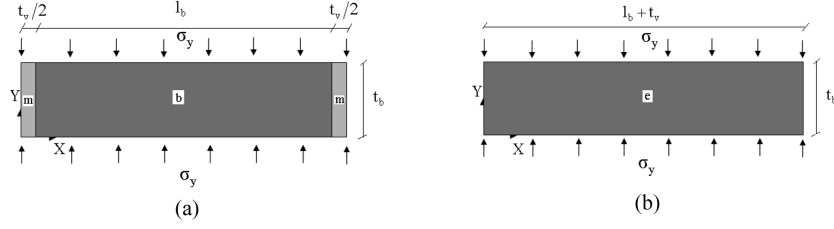


Fig. 8 Steps in the process of homogenization

$$\begin{aligned}\delta_e^y &= \delta_b^y = \delta_v^y \\ \Rightarrow \varepsilon_b^y &= \varepsilon_v^y = \varepsilon_e^y\end{aligned}\quad (18)$$

$$\begin{aligned}\delta_e^x &= \delta_b^x = \delta_v^x \\ \Rightarrow \varepsilon_e^x(l_b + t_v) &= \varepsilon_b^x l_b + \varepsilon_v^x t_v\end{aligned}\quad (19)$$

That

$$\varepsilon_e^x = -\nu_e^{yx} \varepsilon_e^y, \quad \varepsilon_b^x = -\nu_b \varepsilon_b^y, \quad \varepsilon_v^x = -\nu_m \varepsilon_v^y\quad (20)$$

By combining Eqs. (18), (19) and (20)

$$\nu_e^{yx} = (\nu_b l_b + \nu_m t_v) / (l_b + t_v)\quad (21)$$

Based on Betti's law

$$\nu_e^{xy} = (E_e^x / E_e^y) \nu_e^{yx}\quad (22)$$

Where

$$E_e^x = (E_b E_m (l_b + t_v)) / (E_b t_v + E_m l_b)$$

$$E_e^y = (E_b l_b + E_m t_v) / (l_b + t_v)$$

According to the compatibility of deformations in Figs. 7(b) and 7(c), results in

$$\begin{aligned}\delta_p^x &= \delta_e^x = \delta_h^x \\ \Rightarrow \varepsilon_e^x &= \varepsilon_h^x = \varepsilon_p^x\end{aligned}\quad (23)$$

$$\begin{aligned}\delta_p^y &= \delta_e^y + \delta_h^y \\ \Rightarrow \varepsilon_p^y(t_b + t_h) &= \varepsilon_e^y t_b + \varepsilon_h^y t_h\end{aligned}\quad (24)$$

Where

$$\varepsilon_p^y = -\nu_p^{xy} \varepsilon_p^x, \quad \varepsilon_e^y = -\nu_e^{xy} \varepsilon_e^x, \quad \varepsilon_h^y = -\nu_m \varepsilon_h^x \quad (25)$$

By combining Eqs. (23), (24) and (25)

$$\begin{aligned} \nu_p^{xy} &= (\nu_e^{xy} t_b + \nu_m t_h) / (t_b + t_h) \\ \nu_p^{yx} &= (E_p^y / E_p^x) \nu_p^{xy} \end{aligned} \quad (26)$$

Finally, for determining the equivalent specific weight (γ_p), the steps outlined below are followed. According to the equilibrium of forces resulting from gravity acceleration in Figs. 1(c) and 2, it is concluded that

$$P_1 = P_2 \quad \Rightarrow (l_b + t_v)(t_b + t_h)t_w \gamma_p = l_b t_b t_w \gamma_b + [(l_b + t_v)(t_b + t_h) - l_b t_b] t_w \gamma_m$$

After simplification, results in

$$\gamma_p = \frac{\gamma_b l_b t_b + \gamma_m [(l_b + t_v)(t_b + t_h) - l_b t_b]}{(l_b + t_v)(t_b + t_h)} \quad (27)$$

Similarly, other parameters are determined. Briefly, all the elastic constants related to the equivalent orthotropic homogenous material of masonry are introduced in Table 1.

Table 1 Elastic constants of the equivalent orthotropic homogenous material of masonry

E_p^x	$\frac{E_m [E_b (l_b t_b + t_b t_v + t_h t_v) + E_m l_b t_h]}{(E_b t_v + E_m l_b)(t_b + t_h)}$
E_p^y	$\frac{E_m (E_b l_b + E_m t_v)(t_b + t_h)}{E_b l_b t_h + E_m (l_b t_b + t_b t_v + t_h t_v)}$
E_p^z	$\frac{E_b l_b t_b + E_m [(l_b + t_v)(t_b + t_h) - l_b t_b]}{(l_b + t_v)(t_b + t_h)}$
G_p^{xy1}	$\frac{G_m (G_b l_b + G_m t_v)(t_b + t_h)}{G_b l_b t_h + G_m (l_b t_b + t_b t_v + t_h t_v)}$
G_p^{xy2}	$\frac{G_m [G_b (l_b t_b + t_b t_v + t_h t_v) + G_m l_b t_h]}{(G_b t_v + G_m l_b)(t_b + t_h)}$
G_p^{xy}	$2G_p^{xy1} G_p^{xy2} / (G_p^{xy1} + G_p^{xy2})$
G_p^{yz1}	$\frac{G_m (G_b l_b + G_m t_v)(t_b + t_h)}{G_b l_b t_h + G_m (l_b t_b + t_b t_v + t_h t_v)}$
G_p^{yz2}	$\frac{G_b l_b t_b + G_m (l_b t_b + t_b t_v + t_h t_v)}{(l_b + t_v)(t_b + t_h)}$

Table 1 Continued

G_p^{yz}	$2G_p^{yz1}G_p^{yz2}/(G_p^{yz1} + G_p^{yz2})$
G_p^{xz1}	$\frac{G_m[G_b(l_b t_b + t_b t_v + t_h t_v) + G_m l_b t_h]}{(G_b t_v + G_m l_b)(t_b + t_h)}$
G_p^{xz2}	$\frac{G_b l_b t_b + G_m(l_b t_h + t_b t_v + t_h t_v)}{(l_b + t_v)(t_b + t_h)}$
G_p^{xz}	$2G_p^{xz1}G_p^{xz2}/(G_p^{xz1} + G_p^{xz2})$
v_p^{xy}	$[(E_c^x/E_c^y)t_b(v_b l_b + v_m t_v)/(l_b + t_v) + v_m t_h]/(t_b + t_h)$
$v_p^{\bar{z}y}$	$\frac{v_b l_b t_b + v_m(l_b t_h + t_b t_v + t_h t_v)}{(l_b + t_v)(t_b + t_h)}$
$v_p^{\bar{z}x}$	$\frac{v_b l_b t_b + v_m(l_b t_h + t_b t_v + t_h t_v)}{(l_b + t_v)(t_b + t_h)}$

2.4 Comparison with numerical results

Most of the existing methods regarding homogenization of masonry materials are very complicated (Milani *et al.* 2007). The suggested process in the previous sections for establishment of analytical equations for homogenization of unreinforced brick walls is a simple and applicable method. At this stage, it is necessary to investigate the accuracy of proposed equations through detailed modeling. So, three cases including in-plane loading of solid unreinforced brick walls, in-plane loading of perforated unreinforced brick walls and out-of-plane loading of unreinforced brick walls are evaluated. The proposed method can be generalized to every wall with any kind of arrangement that is, homogenization can be performed in the façade and thickness of the walls. Afterwards, some samples are represented.

Here, unreinforced brick walls in two cases of detailed and homogenized are modeled and analyzed in ANSYS nonlinear finite element software. In detailed cases, the mechanical and geometrical properties of bricks and bed and head joints of mortar are considered entirely. In homogenized cases, masonry materials are replaced with an equivalent orthotropic homogeneous material according to the suggested equations in Table 1. In the walls under study, bricks length, width and thickness are 22, 10 and 6 centimeters, respectively. The thickness of horizontal and vertical joints of mortar is 2 cm. Based on the masonry codes, walls made of bricks shall be constructed in such a way that the vertical joints do not fall in one line and thoroughly be filled with mortar.

For in-plane loading, a horizontal tie beam is placed at the top and bottom of walls, the walls are under gravity load, and their weight; lateral loading is then applied to the top of them. In out-of-plane loading, a horizontal tie beam is placed at the bottom of walls; uniform lateral pressure is then applied perpendicular to the plane of walls. The purpose is to compare the stiffness values, the distribution of deformations and stresses, etc in two cases of detailed and homogenized.

2.4.1 Solid unreinforced brick walls under in-plane loading

The parameters under study in this part were consisted of wall aspect ratio ($L/H = 0.7, 1, 1.3, 1.6$ where $H = 3$ m), the proportion of elastic modulus of mortar to brick ($E_m/E_b = 0.1, 0.25, 0.35, 0.5, 0.8$ where $E_b = 2000$ MPa) and the element mesh size (2 cm to 80 cm).

It is necessary to point out here that in detailed modeling, it is not possible to use mesh size bigger than a certain value, since all the bricks and bed and head joints of mortar should be included entirety. However, in the homogenized modeling, there is no such limitation and it is possible to enlarge the size of meshes as much as needed according to the desired accuracy. Therefore, it is decided to select 2 cm to 80 cm mesh size for homogenized modeling. However, for detailed modeling only 2 cm mesh size is applicable.

For instance, a wall is considered with aspect ratio of 1 to 3 under gravity pressure and lateral force of 0.5 MPa and 58 kN, respectively, where 2 cm elements are used for modeling of it in two cases. These wall material properties are as follows (Tasnimi 2004, 2005):

$$\begin{aligned} \text{Properties of brick:} \quad & E_b = 2000 \text{ MPa}, \quad \nu_b = 0.15, \quad \rho_b = 1700 \text{ (kg/m}^3\text{)} \\ \text{Properties of mortar:} \quad & E_m = 700 \text{ MPa}, \quad \nu_m = 0.2, \quad \rho_m = 2100 \text{ (kg/m}^3\text{)} \end{aligned}$$

Equivalent orthotropic homogenous material properties resulting from the suggested equations in Table 1:

$$\begin{aligned} E_p^x &= 1474, \quad E_p^y = 1326.9, \quad E_p^z = 1593.8 \text{ MPa} \\ G_p^{xy} &= 596.87, \quad G_p^{yz} = 620.8, \quad G_p^{xz} = 659.62 \text{ MPa} \\ \nu_p^{xy} &= 0.156, \quad \nu_p^{yz} = 0.138, \quad \nu_p^{xz} = 0.153, \quad \rho_b = 1825 \text{ (kg/m}^3\text{)} \end{aligned}$$

The distribution of deformations and stresses are shown in Figs. 9, 10, 11 and 12 at the end of the loading in the two cases.

With regard to these figures, in Table 2, the maximum value of deformations and stresses in two cases of detailed and homogenized are given as well as the errors resulting from the homogenization process.

The results of the analyses for three walls were similar to this wall but with different aspect ratios

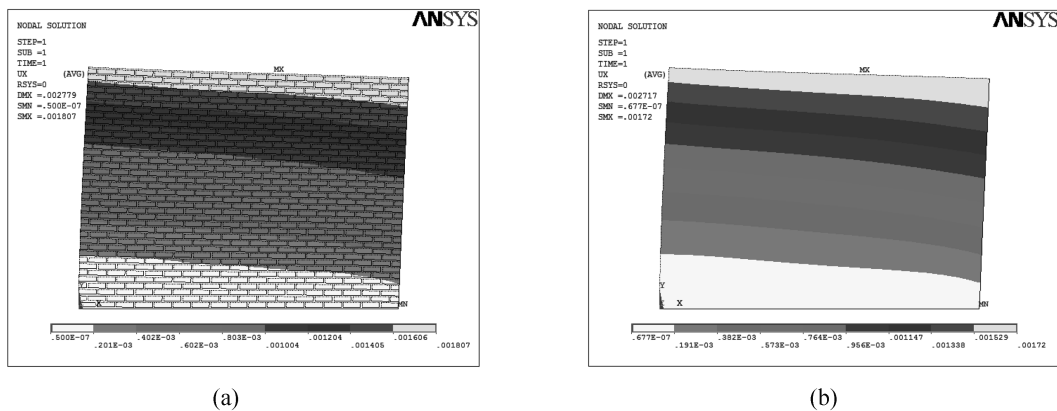
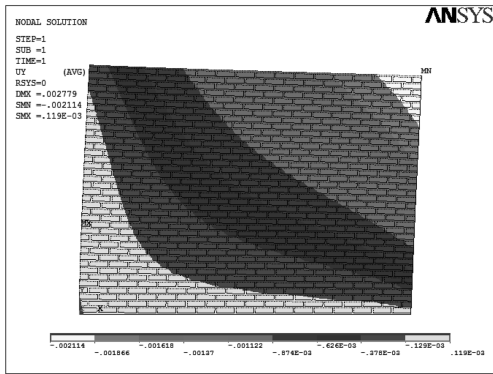
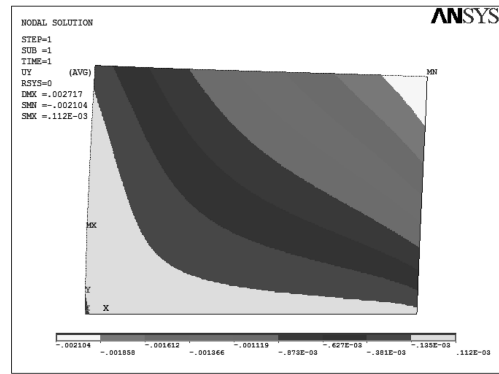


Fig. 9 Distribution of horizontal deformation in two cases of (a) detailed and (b) homogenized

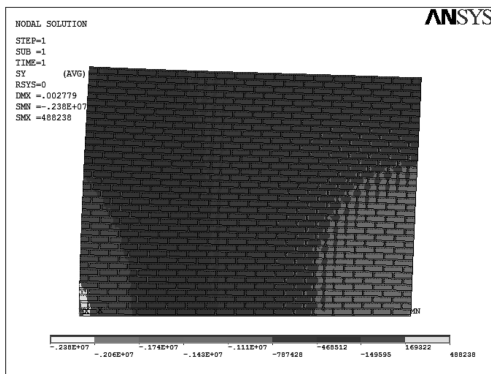


(a)

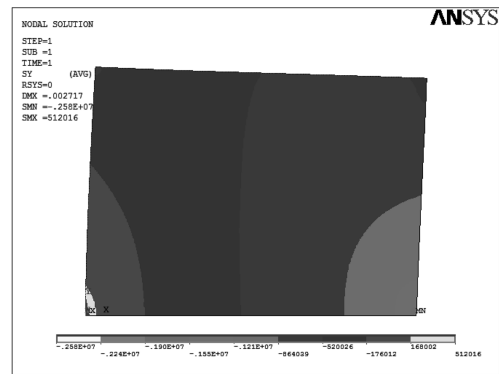


(b)

Fig. 10 Distribution of vertical deformation in two cases of (a) detailed and (b) homogenized

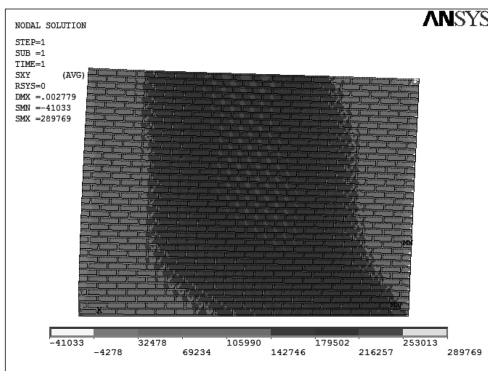


(a)

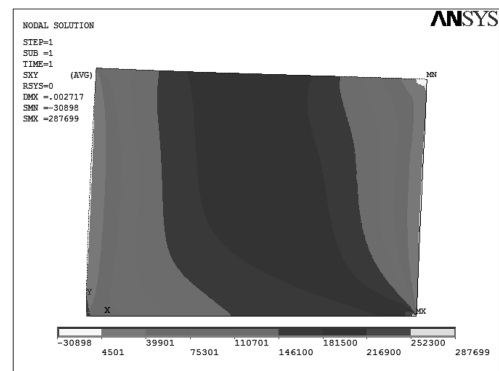


(b)

Fig. 11 Distribution of normal stress in two cases of (a) detailed and (b) homogenized



(a)



(b)

Fig. 12 Distribution of shear stress in two cases of (a) detailed and (b) homogenized

($L/H = 0.7, 1, 1.6$) and under gravity pressure of 0.5 MPa and lateral load of 16 kN, 34 kN, 84 kN, respectively, are presented in Table 3.

Based on Tables 2 and 3, it is seen that the errors resulting from homogenization are less than 10% and negligible for different parameters in all of the walls. Then, the results of the most important parameter, i.e., errors resulting from calculation of stiffness in homogenization process according to the proposed equations, are investigated briefly.

According to the loading and boundary conditions of the walls under study, it seems that in shear

Table 2 Comparison of the results of analyses in two cases of detailed and homogenized

Comparison		Detailed	Homogenized	Error (%)
Lateral deformation (mm)		1.807	1.72	4.81
Vertical deformation (mm)	Positive	0.119	0.112	5.88
	Negative	2.114	2.104	0.47
Normal stress (MPa)	Tension	0.488	0.512	4.87
	Compression	2.38	2.58	8.4
Shear stress (MPa)		0.29	0.288	0.71

Table 3 Comparison of the results of analyses in two cases of detailed and homogenized for different aspect ratio of the walls

Comparison	Error (%)		
	$L/H = 0.7$	$L/H = 1$	$L/H = 1.6$
Lateral deformation (mm)	2.25	3.58	5.46
Vertical deformation (mm)	Positive	3.15	4.95
	Negative	0.24	0.33
Normal stress (MPa)	Tension	5.3	5.17
	Compression	8.63	8.64
Shear stress (MPa)	7.74	2.64	2.81

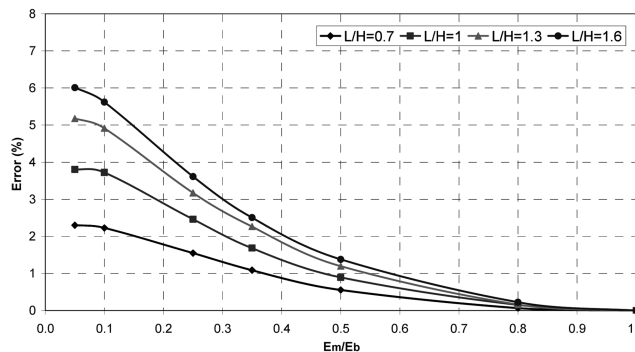


Fig. 13 The errors due to homogenization in calculation of walls stiffness

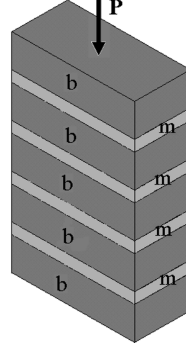


Fig. 14 The masonry panel used in the compression test

deformations, we have the case as shown in Fig. 4. Thus, by taking $G_p^{xy} = G_p^{xy1}$ for brick walls with 2 cm mesh size and different proportions of L/H and E_m/E_b , the errors resulting from homogenization in estimation of walls stiffness, are shown in Fig. 13. It is clear that with an increase in E_m/E_b and approaching to one, masonry materials become homogeneous and homogenization process errors will decrease.

Fig. 13 shows that for different proportions of L/H and E_m/E_b , the errors resulting from homogenization are less than 10% in the all cases and quite insignificant. These errors can be related to the simple hypotheses used in the establishment of equations and incompleteness of used element in homogenization calculations (see Fig. 1) on the edges of walls.

With regard to the special conditions of mortar in a brick wall and the effects of different factors for example, environment conditions, curing method, etc on the mechanical properties of it, for determination of mortar modulus of elasticity (E_m) in a brick wall, it is possible to provide masonry panels for applying compression test according to ASTM C1314 standard, on condition that these panels are held in the conditions similar to the brick wall. Because it shows the real conditions of masonry wall and outcome parameters based on tests only on mortar specimens is not accurate (Gabor *et al.* 2006a, b).

With regard to the equilibrium of forces in Fig. 14, it is concluded that

$$\begin{aligned} P_p &= P_b = P_m & \Rightarrow \sigma_p &= \sigma_b = \sigma_m \\ \Rightarrow \varepsilon_p &= (E_m/E_p)\varepsilon_m, & \varepsilon_b &= (E_m/E_b)\varepsilon_m \end{aligned} \quad (28)$$

According to the compatibility of deformations in Fig. 14, results in

$$\begin{aligned} \delta_p &= \sum_{i=1}^r \delta_{b_i} + \sum_{j=1}^s \delta_{m_j} \\ \Rightarrow \varepsilon_p h_p &= \varepsilon_b \sum_{i=1}^r h_{b_i} + \varepsilon_m \sum_{j=1}^s h_{m_j} \end{aligned} \quad (29)$$

Where h_p , h_b , h_m , r and s parameters show panel height, brick thickness, mortar joint thickness, number of bricks and mortar joints, respectively. By combining Eqs. (28) and (29), leads to

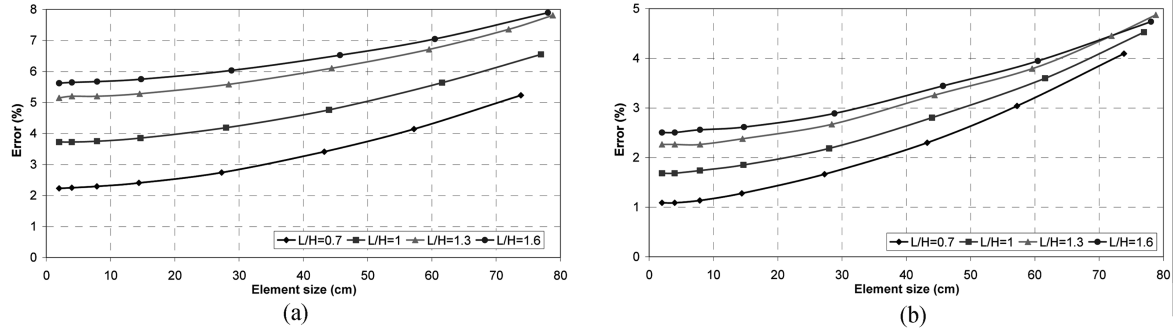


Fig. 15 The errors due to homogenization in calculation of the walls stiffness in two cases of (a) $E_m/E_b = 0.1$ and (b) $E_m/E_b = 0.35$

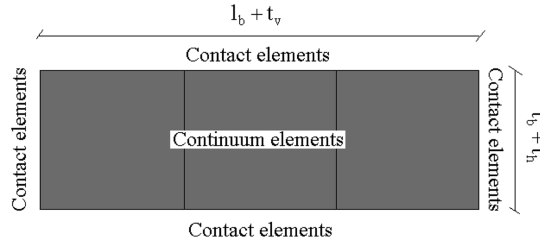


Fig. 16 The maximum element size for considering the all damage modes of a brick wall

$$E_m = E_p E_b \sum_{j=1}^s h_{m_j} / \left(E_b h_p - E_p \sum_{i=1}^r h_{b_i} \right)$$

Elastic modulus of panel (E_p) is determined from measurements of compression test:

$$E_p = \sigma_p / \varepsilon_p = (P/A_p) / (\delta_p/h_p) = (Ph_p) / (A_p \delta_p)$$

Since it is possible to enlarge the elements used in meshing within the homogenized model, in Fig. 15 for brick walls with $E_m/E_b = 0.1, 0.35$ and different L/H , the effect of increase in the element size on the error in calculation of walls stiffness is examined.

According to Fig. 15, it is concluded that the effect of enlarging the element size from 2 cm to 80 cm (which is used in actual cases) in the increase of error is little and the errors due to homogenization in calculation of the walls stiffness constantly are less than 10% which is negligible. Thus, it is possible to preserve the accuracy and decrease the number of elements on the wall façade up to 1600 times more than the number of elements in detailed case that results in the remarkable increase in analysis speed. Therefore, the proposed approach has made applicability in the elastic analysis of a whole masonry building.

On the other hand, in nonlinear analyses, in spite of the fact that the element size can increase up to 8 cm and the number of elements decreases till 16 times in the façade, it is possible to simulate all the existing failure modes in a wall. Because, according to Figs. 1(b) and 16, inside

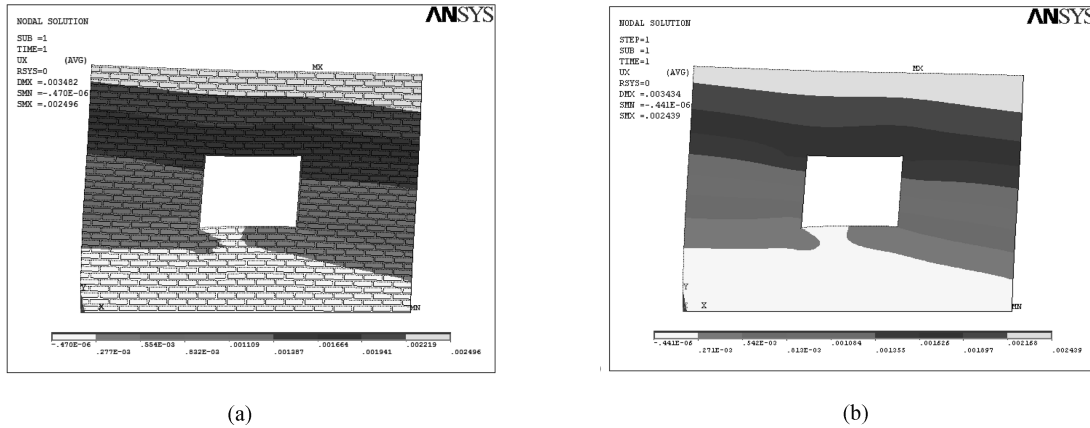


Fig. 17 Distribution of horizontal deformation in a perforated wall in two cases of (a) detailed and (b) homogenized

Table 4 The errors due to homogenization in stiffness calculation of the perforated walls

L/H	Error in stiffness (%)	
	Door Opening	Window Opening
1.3	2.5	2.34
1.6	2.68	2.5

these 8 cm elements, it is possible to use continuum failure models and for considering the sliding, opening, and closing of joints, we can use contact elements on their edges (Yi *et al.* 2006).

2.4.2 Perforated unreinforced brick walls under in-plane loading

Unreinforced brick walls in many cases possess some openings, formed as a result of architectural obligations and usage, such as door, window, etc, which can significantly affect the performance of these walls (Shariq *et al.* 2008). Here, brick walls with $E_m/E_b = 0.35$ and aspect ratios of 1.3 and 1.6, that have openings like door and window are studied. For instance, in Fig. 17, the distribution of lateral deformation of a brick wall with $L/H = 1.3$ accompanied with the window opening under gravity pressure of 0.5 MPa and lateral load of 58 kN is shown.

The errors resulting from homogenization in determination of perforated walls stiffness are given briefly in Table 4. Table 4 shows that although the opening exists in the walls, the prediction of suggested equations for homogenization of walls is acceptable.

2.4.3 Unreinforced brick walls under out-of-plane loading

Here, a wall with $E_m/E_b = 0.35$ and $L/H = 0.7$ in two cases of detailed and homogenized under lateral pressure of 1300 (N/m²) was analyzed. According to Fig. 18, it is seen that the error resulting from homogenization in wall stiffness is very little and is equal to 0.26% which proves the correctness of proposed equations in out-of-plane loading.

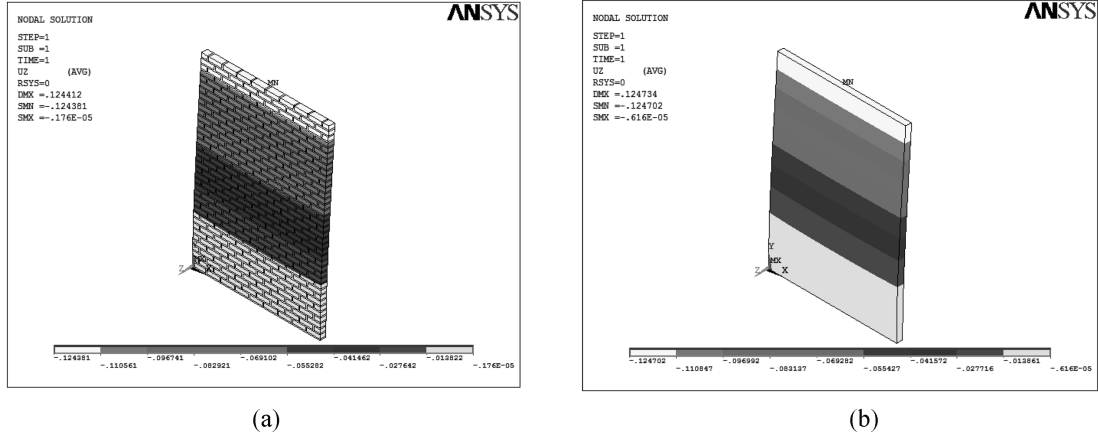


Fig. 18 Distribution of horizontal deformation in the wall under out-of-plane loading in two cases of (a) detailed and (b) homogenized

2.4.4 Homogenization of brick walls in façade and thickness

The process and hypotheses used in the establishment of analytical equations for unreinforced brick wall homogenization in façade is extensible to the thickness for every wall with any kind of arrangement. For instance, a wall is considered with $E_m/E_b = 0.35$ and $L/H = 1$ that is heterogeneous in thickness similar to Fig. 19.

Homogenization of this wall is carried out in three steps which are shown in Fig. 20.

For brick and mortar with the following properties, the equivalent orthotropic homogeneous material at every step according to Fig. 20 is introduced in Table 5.

Properties of brick: $E_b = 2000 \text{ MPa}$, $\nu_b = 0.15$, $\rho_b = 1700 \text{ (kg/m}^3\text{)}$

Properties of mortar: $E_m = 700 \text{ MPa}$, $\nu_m = 0.2$, $\rho_m = 2100 \text{ (kg/m}^3\text{)}$

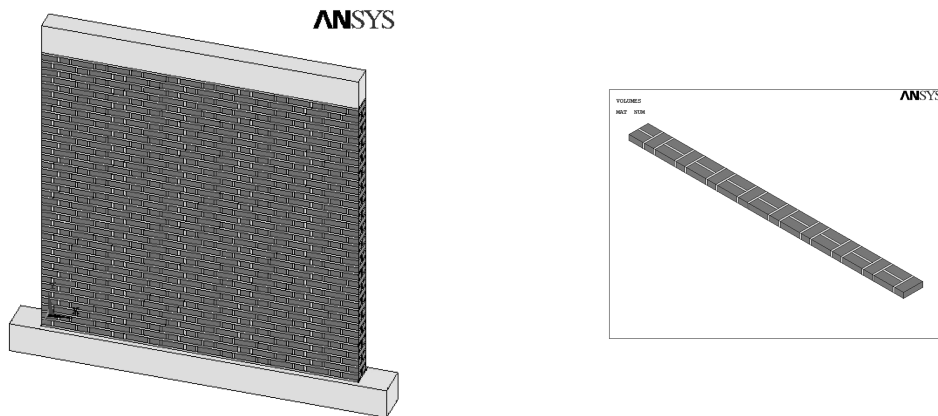


Fig. 19 The 3D wall under study

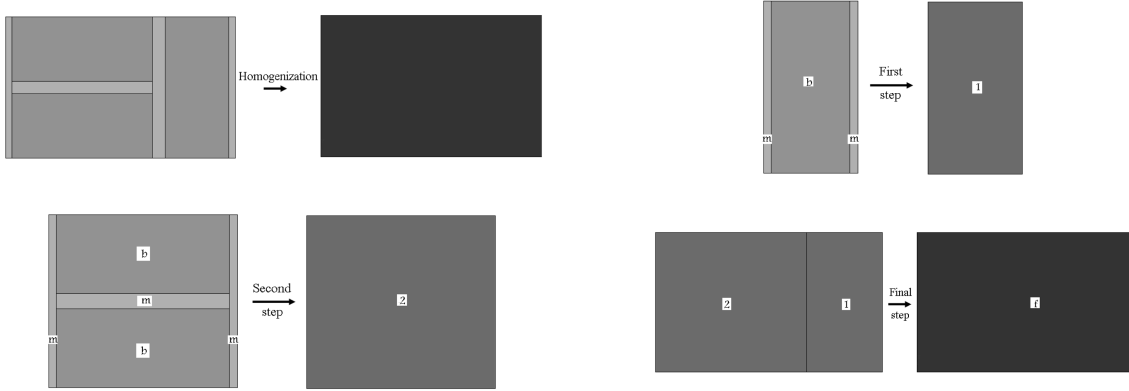


Fig. 20 Steps of homogenization of the 3D wall

Table 5 The equivalent orthotropic homogeneous material properties in every step

Homogenization	Material 1	Material 2	Final material
E_p^x (Mpa)	1320.5	1403.6	1374.8
E_p^y (Mpa)	1285.8	1269.9	1275.2
E_p^z (Mpa)	1512.5	1428	1456.2
G_p^{xy} (Mpa)	555.14	569.2	564.45
G_p^{yz} (Mpa)	595.45	574.25	581.4
G_p^{xz} (Mpa)	604.72	607.31	606.7
ν_p^{xy}	0.152	0.16	0.157
ν_p^{yz}	0.143	0.144	0.144
ν_p^{xz}	0.147	0.157	0.154

In order to calculate the specific gravity of an equivalent orthotropic homogeneous material, similar to Eq. (27), yields to

$$\begin{aligned}
 V_p &= (l_b + b_b + 2t_v)l_b(t_b + t_h) & V_b &= 3l_b b_b t_b \\
 \gamma_p &= (\gamma_b V_b + \gamma_m (V_p - V_b)) / V_p
 \end{aligned}
 \tag{30}$$

Thus, the equivalent specific gravity is obtained as $\gamma_p = 1850$ (kg/m³).

For this wall under its weight and gravity compression of 0.5 MPa and lateral load of 68 kN, the lateral deformation in two cases of detailed and homogenized are shown in Fig. 21.

Fig. 21 shows that the error resulting from homogenization in wall stiffness is 2.53% and negligible. If in this wall, the arrangement of sequential courses of brickwork is changed according to Fig. 22, the result of analysis is given in Table 6 under the title of ‘‘Pattern 2’’.

It is concluded that with this alteration in arrangement, a slight error of 2.51% will occur between two approaches, homogenized and detailed. For walls with different conditions, similar results are

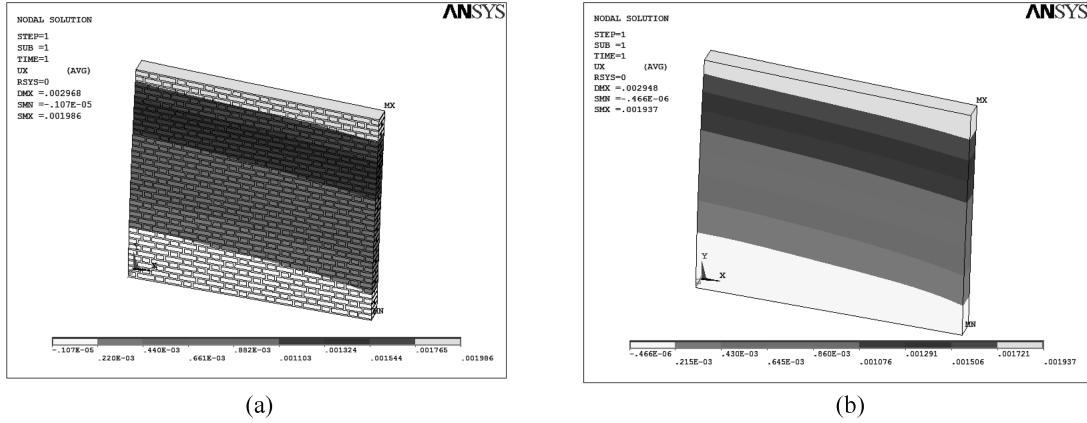


Fig. 21 Distribution of horizontal deformation in the 3D wall in two cases of (a) detailed and (b) homogenized

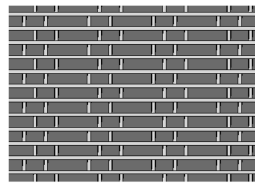


Fig. 22 Change in brickwork sequential courses

Table 6 The errors due to homogenization in calculation of the 3D walls stiffness

Approximate L/H	Error in stiffness (%)	
	Pattern 1	Pattern 2
0.7	1.68	1.43
1	2.53	2.51

obtained which are given in Table 6. Therefore, the recommended method in homogenization of 3D brick walls with heterogeneity in thickness gives acceptable accuracy and has considerable benefits.

3. Modeling of diagonal compression test

After homogenization of brick walls and determination of their stiffness with high accuracy, their strength is evaluated here. For this purpose, the diagonal compression test according to ASTM E519 is considered. This test can simply and efficiently be used for specifying the diagonal cracking strength in brick walls and simulation of the diagonal cracking failure mode which is the most common in-plane damage mode in unreinforced brick walls. This test method covers the determination of the diagonal tensile or shear strength of 1.2 by 1.2 m (4 by 4 ft) masonry

assemblages by loading them in compression along one diagonal, thus causing a diagonal tension failure with the specimen splitting apart parallel to the direction of the load.

In a lot of researches on the analysis and assessment of different methods for strengthening of unreinforced masonry walls such as the use of fiber reinforced polymer sheets (FRP), using FRP rods, etc; the diagonal compression test is used in order to observe the damage mode and measure the stiffness, ultimate strength and deformation capacity of masonry panels after retrofitting, then by comparing their results with an unretrofitted case, the performance of these methods becomes characterized (Hamid *et al.* 2005, Prota *et al.* 2006, Turco *et al.* 2006, Valluzzi *et al.* 2002).

In FEMA 356, for calculation of the load bearing capacity of unreinforced brick walls in the case of diagonal failure, the following equation is introduced

$$V_{dt} = f'_{dt} A_n \left(\frac{L}{h_{eff}} \right) \sqrt{1 + \frac{f_a}{f'_{dt}}} \tag{31}$$

Where L , h_{eff} and A_n are geometrical parameters, f_a is axial compressive stress due to gravity loads and f'_{dt} is masonry diagonal cracking strength which is obtained from diagonal compression test of masonry panels.

Masonry panels under the test have a shape similar to a square and their width and length are about 1.2 meters and have preferred thickness. The selected measures for the dimensions of specimens are the minimum values so that the specimens become perfect representatives of a real wall. Steel loading shoes at the top and bottom corners of panels must have the minimum bearing length of 15 cm in any direction with the masonry panels so that stress concentration and local failure does not occur at the loading corners and the failure occurs in the form of propagated cracks within bricks or mortar joints along the diagonal under pressure.

For nonlinear modeling of brick panels, it is suitable to use Drucker-Prager or Willam-Warnke failure criteria (Betti and Vignoli 2008a, b, Gabor 2006a, b, Kappos *et al.* 2002, Pallarés *et al.* 2006). Drucker-Prager failure model is applicable to granular (frictional) material such as soil, rock, masonry material, and concrete, and according to Fig. 23 uses the outer cone approximation to Mohr-Coulomb law.

Firstly, the experimental work by Gabor *et al.* (2006) is considered. After numerical modeling and including brick and mortar separately and comparing it with the experimental results, according to Fig. 24, it became clear that Drucker-Prager failure criterion is able to simulate the nonlinear behavior of brick panels. Therefore, this model is used in the rest of this research. The parameters under study in this section are mesh density, mortar type (weak to strong mortars).

In the most existing unreinforced brick walls, mortar joints are the weak planes in the set and most of the damages and decays are focused at these regions (Abdou *et al.* 2006, ElGawady *et al.*

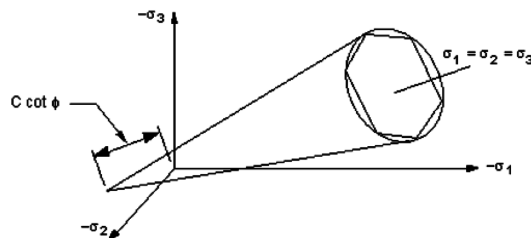


Fig. 23 Mohr-Coulomb and Drucker-Prager failure models in the space of principal stresses

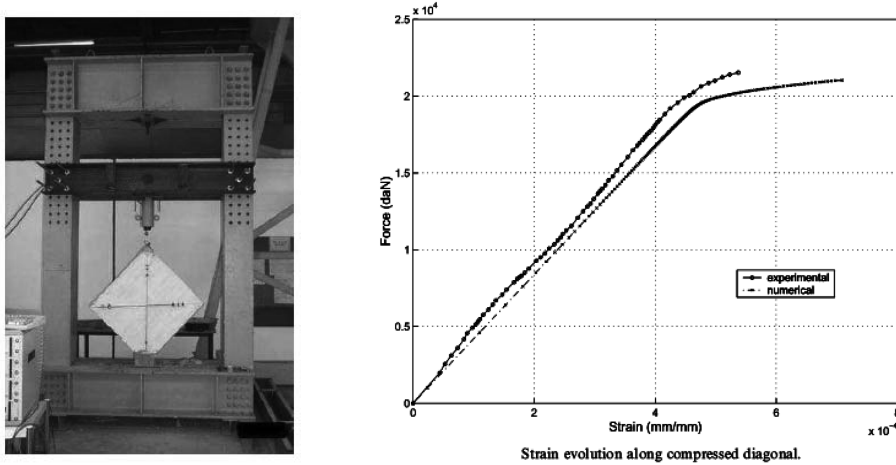


Fig. 24 Comparison of the unreinforced brick panel behavior under diagonal compression in two cases of experimental and detailed numerical (Gabor *et al.* 2006)

2007, Gabor *et al.* 2006a, b). In detailed nonlinear modeling of a brick wall, the linear and nonlinear properties of brick and mortar joints must be considered separately in the model. For the sake of simplicity, applicability and conservativeness of the issue, it is discussed here that if brick walls according to the proposed analytical equations in section 2 become homogeneous then, the nonlinear properties of mortar joints are assigned to this homogenized material, how much error is in estimation of wall strength?

The main idea in the suggested model is that in a brick wall with weak mortar joints, cracks primarily occur in mortar joints and are limited to these regions. However, in the proposed model, cracks can occur in every place in the wall. Since there are many mortar joints in the wall and they exist in every region, the considered hypothesis seems logical. Moreover, it is clear that by improving the mortar and having more similarities with brick from the viewpoint of nonlinear properties, the accuracy of this hypothesis increases. Thus, in order to study the brick walls diagonal cracking mode, diagonal compression is applied to masonry panels in two cases of detailed and homogenized then in addition to stiffness, the ultimate strength is also compared and the accuracy of homogenization is investigated.

The length, width and thickness of masonry panels are 126, 126 and 10 cm, respectively, and are composed of materials with the linear and nonlinear (i.e., cohesion strength and internal friction angle) properties given below and illustrated in Table 7 (Tasnimi 2004, 2005).

Properties of brick: $E_b = 2000 \text{ MPa}$, $\nu_b = 0.15$, $c_b = 2.2 \text{ MPa}$, $\phi_b = 42^\circ$

Properties of mortar: $E_m = 700 \text{ MPa}$, $\nu_m = 0.2$

The panels in two cases of detailed and homogenized similar to Fig. 25 are modeled under diagonal compression and the behavior curves are drawn for comparison in Fig. 26.

Fig. 26 shows that the error resulting from homogenization in masonry panels' stiffness is very small and equals 0.34%. Also, in different types of used mortars (weak to strong mortars), the ultimate load bearing capacity of brick panels in homogenous case is smaller than that of detailed case and the error resulting from homogenization in estimation of all panels ultimate strength is less

Table 7 Nonlinear properties of different used mortars

Type of mortar	c_m (MPa)	φ_m
Type 1	0.25	27°
Type 2	0.64	30.5°
Type 3	1.03	33.7°
Type 4	1.42	36.7°
Type 5	1.81	39.4°

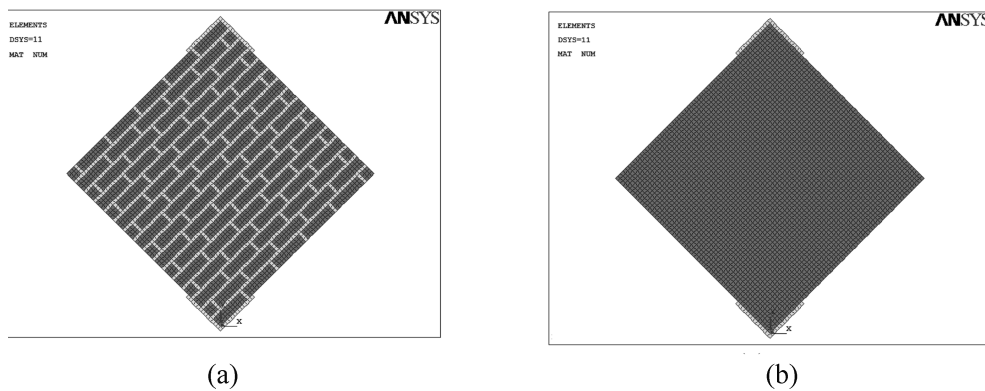


Fig. 25 Modeling of brick panels under diagonal compression in two cases of (a) detailed and (b) homogenized

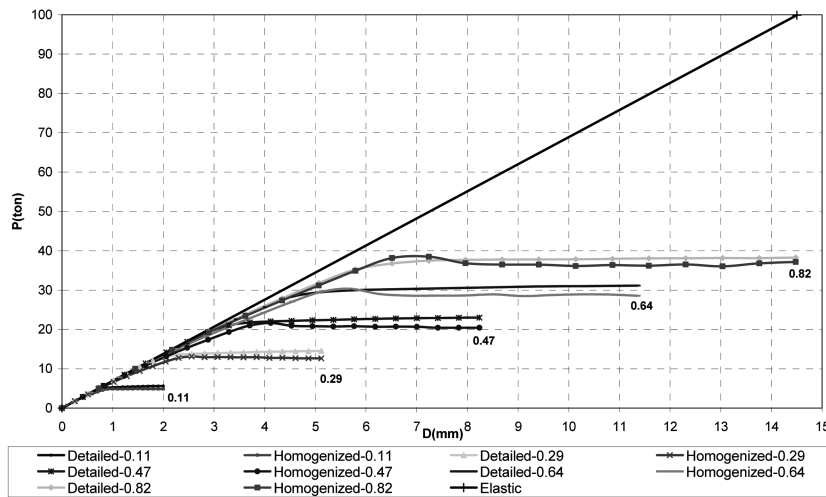


Fig. 26 Force-deformation behavior of the panels along compressed diagonal in two cases of detailed and homogenized for different c_m/c_b

than 10% and negligible. The details are given in Table 8.

Table 8 indicates that by improving the mortar, error decreases. For instance, in Figs. 27 and 28 for mortar type 3, the distribution of damage in panels is presented in two cases of detailed and

homogenized.

In the equivalent plastic strain, the share of all plastic strain components is considered. Figs. 27 and 28 demonstrate that the damage distribution in panels in detailed and homogenized cases is similar. Also, the difference in the maximum equivalent plastic strain in diagonal deformations of 5.4 and 7 mm is insignificant and equals 1.2% and 7.3%, respectively. In other cases, there are similar results.

Table 8 The errors in estimation of panels ultimate load based on the used type of mortar

Type of mortar	Error in strength (%)
Type 1	9.52
Type 2	7.2
Type 3	6.68
Type 4	6.05
Type 5	3.41

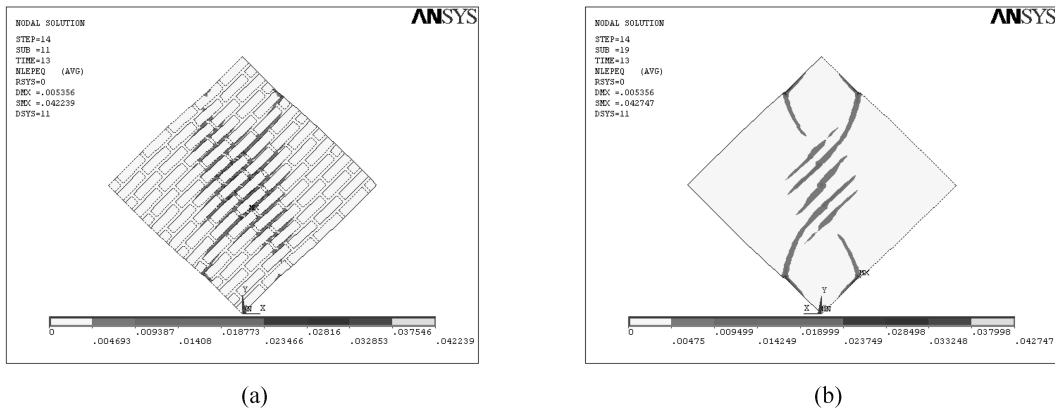


Fig. 27 Distribution of equivalent plastic strain in the panel under diagonal compression in two cases of (a) detailed and (b) homogenized for diagonal deformation of 5.4 mm

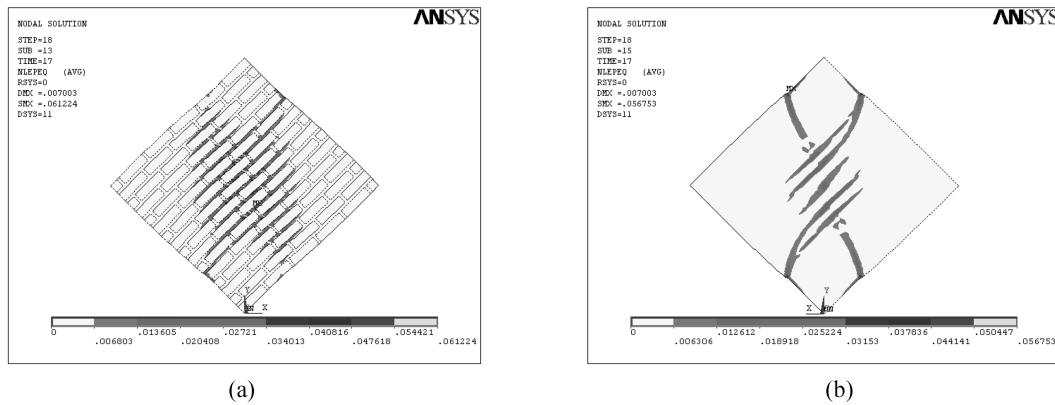


Fig. 28 Distribution of equivalent plastic strain in the panel under diagonal compression in two cases of (a) detailed and (b) homogenized for diagonal deformation of 7 mm

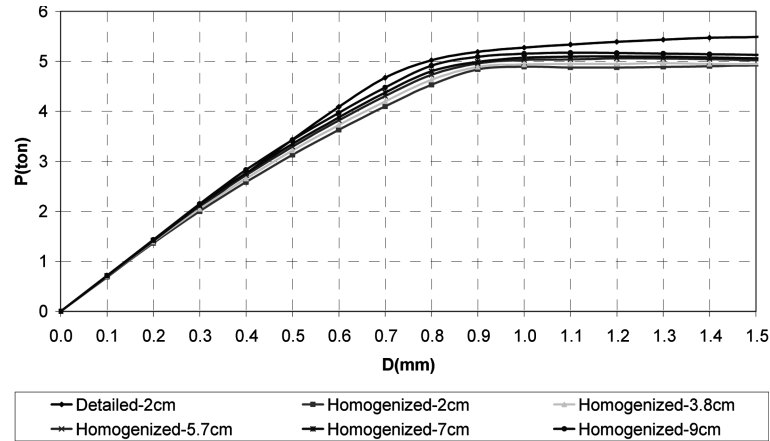


Fig. 29 Force-deformation behavior of the panels along compressed diagonal in two cases of detailed and homogenized for different element sizes

Table 9 The errors due to homogenization in the stiffness and ultimate load of panels

The size of element (cm)	Error in stiffness (%)	Error in strength (%)
2	0.34	9.52
3.8	1.31	8.18
5.7	2.33	6.18
7	2.98	5.4
9	4	4.17

As it was discussed before, one of the advantages of homogenization is the feasibility of increase in the size of elements according to the desired accuracy. Therefore, here, the effect of largeness and smallness of elements in stiffness and ultimate strength of panels is studied. In Fig. 29, for the case of $c_m/c_b = 0.11$ (the weakest mortar), the behavior curves of panels under diagonal compression in two cases of detailed and homogenized (with various element sizes) are drawn.

Based on Fig. 29, the errors resulting from homogenization and enlarging the elements are presented in Table 9.

Table 10 shows that with an increase in the size of elements until approximately 9 cm and simultaneously decrease in the number of elements until approximately 20 times in the panel façade, the error in estimation of unreinforced brick wall stiffness and ultimate strength is still less than 10% and negligible.

4. Establishment of a finite element model for unreinforced brick walls

Now, for simulation of all the damage modes of unreinforced brick walls according to Fig. 30 and accurate estimation of their strength, with regard to Figs. 1 and 2, the finite element model shown in Fig. 31 is proposed.

In this model, according to Fig. 31, bricks are enlarged and entitled “brickwork units”. The

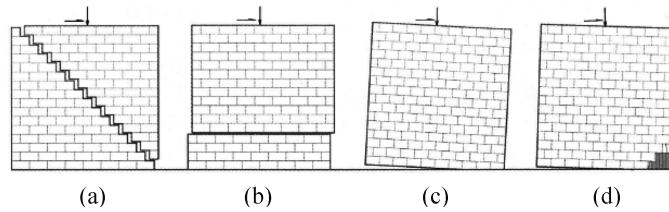


Fig. 30 In-plane failure modes of unreinforced brick walls (a) shear failure, (b) sliding failure, (c) rocking failure, (d) flexure failure (ElGawady *et al.* 2007)

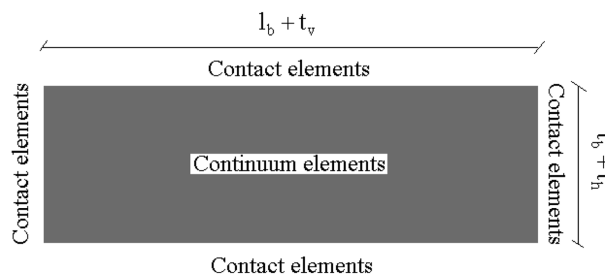


Fig. 31 The proposed Finite element model for unreinforced brick walls

thickness of a brickwork unit is equal to the brick thickness plus the horizontal mortar joint thickness and its length is equal to the brick length plus the vertical mortar joint thickness. As mentioned earlier, with regard to the orthotropic nature of masonry materials in a brick wall, the material constituting these brickwork units is considered orthotropic that its elastic properties are determined in accordance with the established equations in section 2. For nonlinear modeling of brickwork units and considering brick cracking and masonry crushing, Drucker-Prager failure criterion is used.

Frictional contact elements are placed in between the brickwork units. They are able to simulate the sliding, opening, and closing of mortar joints. Primarily, they are in a stuck state and if their shear stress exceeds the frictional strength plus cohesion strength of mortar joints, the brickwork units slide on each other. These elements transfer compression between the brickwork units and open under tension.

In this modeling, various nonlinear models including the material and element nonlinearity are considered. With regard to using the contact elements between the brickwork units and for reduction in convergence problems and prevention of rigid body motion, weak springs are placed between the brickwork units that are in touch with each other. These springs have stiffness an order of very small relative to masonry materials stiffness around. These connections between surfaces that are in touch with each other result in the stability of the system and do not have any effect on the results.

5. Comparison with experimental results

Now for studying the performance of proposed model in anticipation of the damage pattern and ultimate strength of unreinforced brick walls, two specimens from Vermeltfoort's tested walls under shear and compression (Chaimoon and Attard 2007), in ANSYS nonlinear finite element software

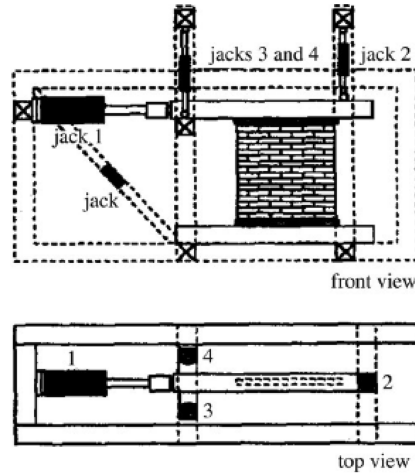


Fig. 32 The shear wall test setup (Chaimoon and Attard 2007)

are modeled. These specimens, according to Fig. 32, had length, height and thickness of 990, 1000 and 98 millimeters, respectively, and consisted of 16 brickwork courses that the two of them were clamped at the top and bottom steel shoes. The bricks were solid clay with dimensions $204 \times 98 \times 50$ mm and a 10 mm thick mortar joint was used. The mortar was low strength and had a composition of 1 part cement to 2 parts lime to 9 parts sand, by volume. Two different vertical pre-compression distributed loads of 1.21 and 2.12 MPa were first applied to the top of walls. Monotonically increasing horizontal loading was then applied to the top of any wall through a horizontal upper beam. Three vertical jacks were used to keep the upper beam in a horizontal position (see Fig. 32).

In this test, with regard to the high importance of the modeling method of loading conditions, various finite element models have been chosen by different researchers. Lourenco modeled the top boundary with rollers based on the assumption that the top boundary is always horizontal and precluding any vertical movement while Giambanco *et al.* introduced a spring between the rollers and the top brick course; Chaiman and Attard applied a layer of soft material placed between the rollers and the horizontal loading beam (Chaimoon and Attard 2007). In this research, the top boundary of the wall is constrained in a manner that vertical movement of different points of the wall in that boundary is the same and that boundary remains horizontal during loading.

Geometrical and finite element models of the experimental walls are shown in Fig. 33. The elastic properties of masonry materials are obtained from the test results and are given in Table 10 and are assigned to the brickwork units. Nonlinear properties of the brickwork units including cohesion strength (c), internal friction angle (φ) and dilatancy angle (ψ) are determined from the existing test results. Masonry material compressive strength (f_c) and brick tension strength (f_{tb}) were reported 11 and 2 MPa, respectively, and according to Drucker-Prager failure criterion, we have

$$\sin \varphi = \frac{f_c - f_{tb}}{f_c + f_{tb}}$$

$$c = \frac{1 + \sin \varphi}{2 \cos \varphi} f_{tb} \quad (32)$$

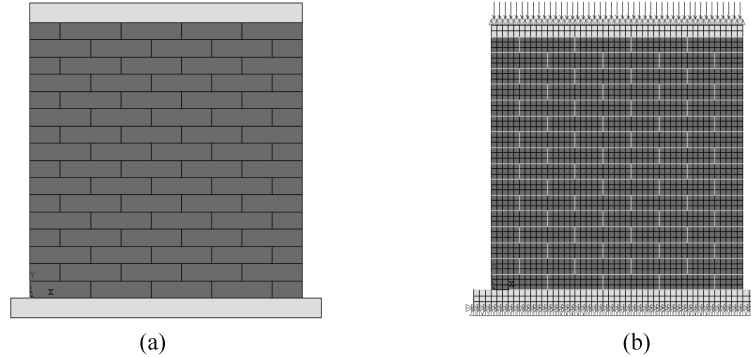


Fig. 33 Geometrical and finite element models for the experimental specimens

Table 10 Elastic properties of the brickwork units

w (MPa)	E (MPa)	ν
1.21	3900	0.11
2.12	3150	0.14

Table 11 Nonlinear properties of the contact elements

w (MPa)	c_m (MPa)	$\tan\phi_m$
1.21, 2.12	0.224	0.75

Hence, c and ϕ are obtained:

$$c = 2.35 \text{ MPa}, \phi = 44^\circ$$

With regard to boundary conditions, the value of ψ is equal to zero.

Also, the nonlinear properties of mortar joints with reference to the mortar joint shear test results as given in Table 11, are taken for contact elements in the finite element model. The selected contact element is CONTA172 which is a 2D 3-node surface-to-surface contact element. With regard to using contact elements between the brickwork units in the proposed finite element model and this point that surfaces which are in touch should recognize each other before the main loading (lateral loading), it is necessary to include preparations in modeling. Because of the presence of compression load on the top of walls, for horizontal joints there is no problem, however, for vertical joints, some actions need to be undertaken. At first step, after modeling the wall and applying the boundary conditions at the bottom of wall and applying the constraints at the top of wall, lateral degree of freedom (DOF) at the first and end of wall is restrained, then compression load is applied to the top of wall. In this state, the surfaces which are in touch in vertical joints, realize each other. In subsequent step, lateral DOF at the first and end of wall is released and then the wall is pushed monotonically increasing until the wall collapses.

According to the experimental observations in Fig. 34 first, the horizontal tension cracks at the top and bottom of walls initiate, then with an increase in lateral deformation, the stepped shear

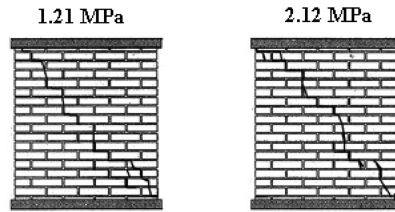


Fig. 34 Experimental crack pattern for each case (Chaimoon and Attard 2007)

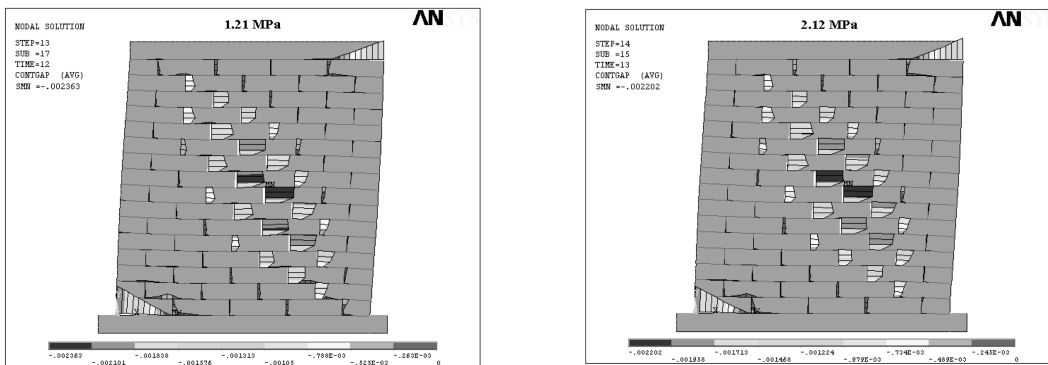


Fig. 35 Distribution of joints opening at the walls failure threshold

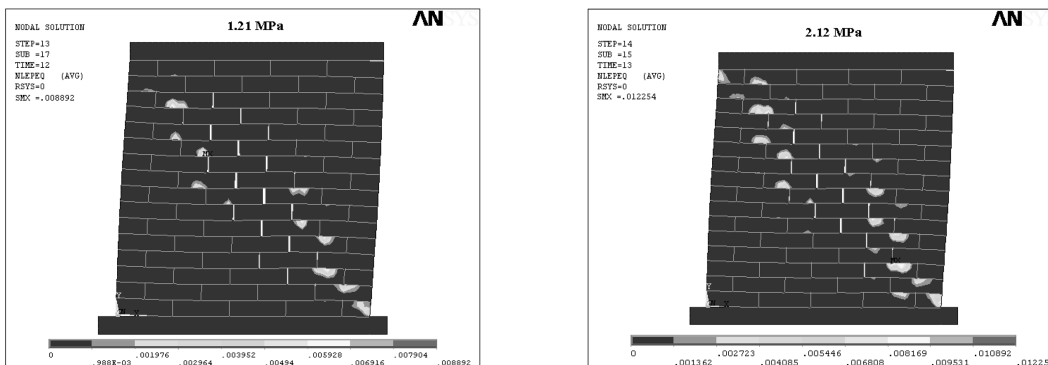


Fig. 36 Distribution of equivalent plastic strain at the walls failure threshold

cracks passing within the mortar joints along diagonal of walls develop and finally lead to the collapse of walls. In some regions, these cracks pass within the bricks and also some crushing in the toe of walls is available.

Figs. 35 and 36 show that the recommended model can foresee well all the damage modes. Opening and sliding of the joints in Fig. 35 is indicative of the tension cracking of walls at the top and bottom and illustrative of the shear cracking band along walls diagonal within mortar joints. The equivalent plastic strain in Fig. 36 is demonstrative of the cracked regions of model (bricks cracking). In equivalent plastic strain, the share of all the plastic strain components is considered. It is clear that in some places of the walls where the plastic strain does not exist, the bricks remain undamaged.

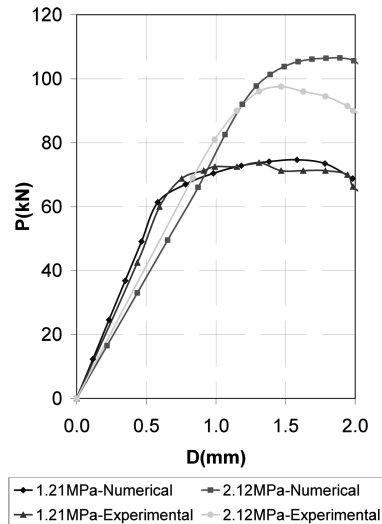


Fig. 37 Force-deformation behavior of the walls in two cases of experimental and numerical

For comparison of the ultimate load bearing capacity of walls in two cases of experimental and numerical, their force-deformation curves are represented in Fig. 37. Because of the presence of contact elements and the effect of their stiffness on the walls deformation values, it is necessary to modify the deformation values which is done in Fig. 37. Since in the ideal case, the stiffness of contact elements must be infinite, because of numerical problems in finite element solution, a large value is chosen for it. Flexure and shear failure are dominant failure modes in unreinforced brick walls and in these cases, the behavior of wall is brittle and is considered as force controlled member (according to FEMA 356). Therefore, exact estimation of the wall strength is very important for the seismic vulnerability assessment of them.

Fig. 37 illustrates that the errors in estimation of the ultimate load bearing capacity of walls in two cases of $w = 1.21$ MPa and $w = 2.12$ MPa are equal to 1.23% and 9.23%, respectively, that are negligible and representative of high ability of the proposed model in forecasting of the failure modes and strength of unreinforced brick walls.

6. Parametric studying

According to the appropriate accuracy of the suggested model, it can be efficiently used for parametric study of effective factors on the unreinforced brick walls performance. These parameters include compression load, mortar type, brick type, etc. Also, if vertical joints in an unreinforced brick wall are not filled with mortar as it is often seen, in modeling, one can set the contact elements in those places with zero cohesion strength and appropriate friction coefficient.

For instance, a common unreinforced brick wall as shown in Fig. 38 with aspect ratio of 1.5 ($H = 2.8$ m) and thickness of 30 cm is considered. The bricks have thickness, width and length of 6, 10 and 22 cm, respectively. Thickness of the horizontal and vertical mortar joints is equal to 2 cm. Properties of the constituent materials of wall are as follows (Tasnimi 2004, 2005):

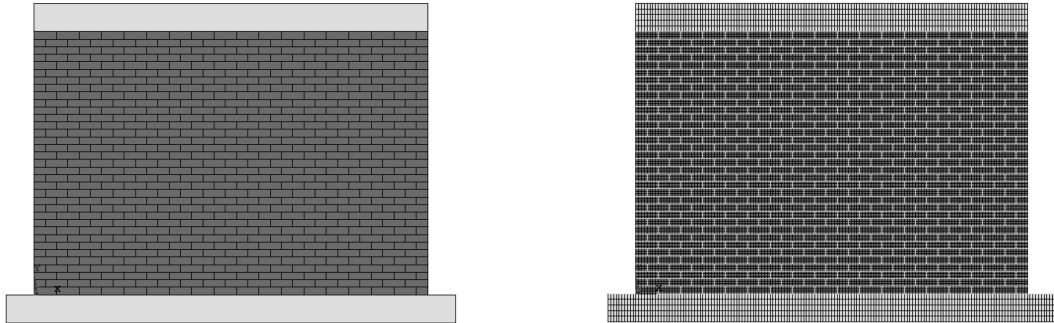


Fig. 38 Geometrical and finite element models of the walls under study

Properties of brick: $E_b = 2000 \text{ MPa}$, $\nu_b = 0.15$, $\rho_b = 1700 \text{ (kg/m}^3\text{)}$, $f_{bt} = 2 \text{ MPa}$
 Properties of mortar: $E_m = 700 \text{ MPa}$, $\nu_m = 0.2$, $\rho_m = 2100 \text{ (kg/m}^3\text{)}$, $c_m = 0.25 \text{ MPa}$, $\tan\phi_m = 0.51$
 Properties of masonry panel: $f_c = 10 \text{ MPa}$

Elastic properties of the brickwork units with reference to the proposed equations are obtained:

$$E_p^x = 1474, \quad E_p^y = 1326.9, \quad E_p^z = 1593.8 \text{ MPa}$$

$$G_p^{xy} = 596.87, \quad G_p^{yz} = 620.8, \quad G_p^{xz} = 659.62 \text{ MPa}$$

$$\nu_p^{xy} = 0.156, \quad \nu_p^{yz} = 0.138, \quad \nu_p^{xz} = 0.153, \quad \rho_v = 1825 \text{ (kg/m}^3\text{)}$$

Nonlinear properties of the brickwork units are determined with regard in Eq. (32):

$$c = 2.2 \text{ MPa}, \quad \phi = 42^\circ$$

Here, the purpose is evaluation of the mortar type (weak to strong mortars) and value of compression load applied to the top of walls, on the performance of them. Different types of mortars are given in Table 12 and the pressure values are 0.5, 1, 1.5 and 2 MPa.

For mortar type 1 and different compression loads, the force-deformation behavior of walls is represented in Fig. 39(a). It is seen that with an increase in compression load, the ultimate strength of walls increases. Since in most of the existing unreinforced brick walls, mortar joints are weak planes of the set and most of the damages and deteriorations of walls are focused in those places (Abdou *et al.* 2006, ElGawady *et al.* 2007, Gabor *et al.* 2006a, b); with an increase in compression, the frictional strength of joints increases and leads to an increase in the ultimate load bearing capacity of walls. Also in practice, the values of compression loads applied to the top of walls are much lesser than the compressive strength of masonry materials.

For the maximum compression case ($w = 2 \text{ MPa}$), opening and sliding of the joints as well as the

Table 12 Types of used mortars

Type of mortar	c_m (MPa)	$\tan\phi_m$
Type 1	0.25	0.51
Type 2	0.64	0.59
Type 3	1.03	0.67

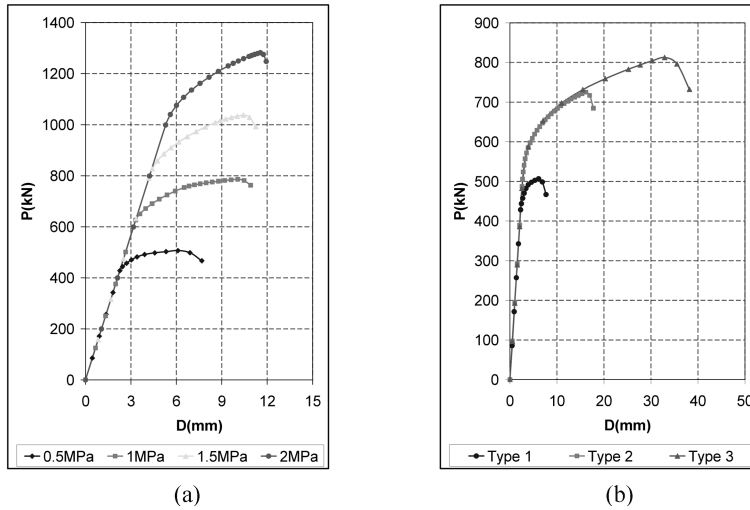


Fig. 39 Force-deformation behavior of the walls: (a) different compression loads and (b) different mortars

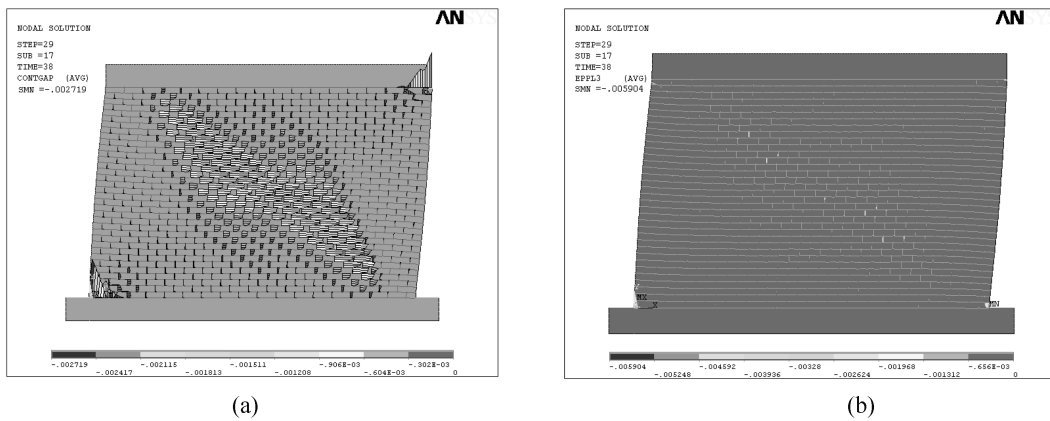


Fig. 40 Distribution of (a) joints opening and sliding (b) principal plastic strain in the wall with $w = 2$ MPa at failure threshold

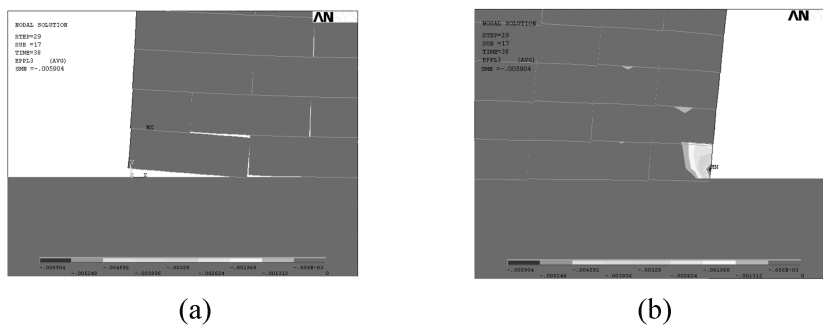


Fig. 41 Heel Rising and toe crushing of the wall

distribution of principal plastic strain are shown in Figs. 40 and 41. It can be seen that the damages are concentrated in joints and bricks remain undamaged with the exclusion of the wall toe.

In Fig. 39(b), for the case of $w = 0.5$ MPa and different types of mortar, the force-deformation curves are drawn. It is obvious that with an improvement in the mortar and increase in its strength parameters, the ultimate load bearing capacity of wall shall increase.

7. Conclusions

The proposed modeling approach in this article can be utilized for applied purposes in stone masonry structures. The only significant disparity lies in the fact that rectangular blocks of stone has been used instead of bricks.

With regard to the large number of existing unreinforced masonry buildings which are vulnerable from a seismic point of view, nonlinear analyses are needed to be performed on this type of buildings, so that, if necessary, their seismic rehabilitation shall be undertaken.

Firstly, a homogeneous orthotropic material was introduced which can be substituted for masonry material (collection of brick and mortar). In different cases such as in-plane and out-of-plane loading, solid and perforated walls, heterogeneity in wall thickness, etc, the proposed homogenization method was investigated and its reasonable accuracy (errors were less than 10%) was confirmed. It was seen that in spite of an increase in element size up to 80 cm in which is being used in actual situations, errors due to the proposed homogenization method were quite negligible. In addition, for evaluating the most common damage mode of walls, namely, diagonal cracking, the diagonal compression test of masonry panels was simulated and the errors obtained from the suggested method in estimation of the ultimate strength were less than 10% and negligible.

Afterwards, a finite element model for assessing the nonlinear behavior of these walls was presented. After comparison with the experimental results, it became obvious that the errors resulting from the proposed procedure in estimation of the ultimate load bearing capacity were less than 10% and insignificant; in addition, the distribution of damages in these walls was predicted satisfactorily.

With regard to the exact estimation of linear and nonlinear characteristics of unreinforced brick walls, such as stiffness, ultimate load bearing capacity, failure pattern, etc, by means of the proposed model, the introduced method can be effectively used for assessing the seismic performance of these types of structures. Stiffness is effective on structure period, deformations and values of earthquake lateral loads. For examination of the structural system sufficiency in carrying applied loads, determining the wall strength is necessary. If the structural system is weak, an accurate prediction of the damage pattern is very helpful in the selection of a suitable strengthening technique.

The proposed nonlinear model is a semi-macro model, with difficulty in applying it to complete masonry buildings. But, from the obvious advantages visualized in the proposed modeling, it can be said that this semi-macro model, with the experience and experimental observations can simply be changed into a macro model. Under some circumstances, if in an unreinforced brick wall with specific geometry and loading, one can predict the cracking paths, the whole wall can be modeled as a continuum medium and contact elements are placed only in the predicted cracking paths. In this case, it is not necessary to set contact elements in the total horizontal and vertical joints, moreover by preserving the precision, complexity of the model and time of the analysis diminishes. At present, the authors of this article are developing simple macro models for unreinforced brick walls in different conditions, these results will be presented in a subsequent article.

References

- Abdou, L., Ami Saada, R., Meftah, F. and Mebarki, A. (2006), "Experimental investigations of the joint-mortar behaviour", *Mech. Res. Commun.*, **33**(3), 370-384.
- American Society for Testing and Materials (ASTM), *Standard Test Method for Compressive Strength of Masonry Prisms, C1314*.
- American Society for Testing and Materials (ASTM), *Standard Test Method for Diagonal Tension (Shear) in Masonry Assemblages, E519*.
- Benedetti, A. and Steli, E. (2008), "Analytical models for shear-displacement curves of unreinforced and FRP reinforced masonry panels", *Constr. Build. Mater.*, **22**(3), 175-185.
- Betti, M. and Vignoli, A. (2008a), "Assessment of seismic resistance of a basilica-type church under earthquake loading: Modelling and analysis", *Adv. Eng. Sof.*, **39**(4), 258-283.
- Betti, M. and Vignoli, A. (2008b), "Modelling and analysis of a Romanesque church under earthquake loading: Assessment of seismic resistance", *Eng. Struct.*, **30**(2), 352-367.
- Chaimoon, K. and Attard, M.M. (2007), "Modeling of unreinforced masonry walls under shear and compression", *Eng. Struct.*, **29**(9), 2056-2068.
- ElGawady, M.A., Lestuzzi, P. and Badoux, M. (2007), "Static Cyclic Response of Masonry Walls Retrofitted with Fiber-Reinforced Polymers", *J. Comp. Constr., ASCE*, **11**(1), 50-61.
- FEMA 356 (2000), *Prestandard for the Seismic Rehabilitation of Buildings*, Federal Emergency Management Agency, Washington, D.C.
- Gabor, A., Bennani, A., Jacquelin, E. and Lebon, F. (2006a), "Modelling approaches of the in-plane shear behaviour of unreinforced and FRP strengthened masonry panels", *Comp. Struct.*, **74**(3), 277-288.
- Gabor, A., Ferrier, E., Jacquelin, E. and Hamelin, P. (2006b), "Analysis and modelling of the in-plane shear behaviour of hollow brick masonry panels", *Constr. Build. Mater.*, **20**(5), 308-321.
- Hamid, A.A., El-Dakhkhni, W.W., Hakam, Z.H.R. and Elgaaly, M. (2005), "Behavior of composite unreinforced masonry-fiber-reinforced polymer wall assemblages under in-plane loading", *J. Compos. Constr., ASCE*, **9**(1), 73-83.
- Kappos, A.J., Penelis, G.G. and Drakopoulos, C.G. (2002), "Evaluation of Simplified Models for Lateral Load Analysis of Unreinforced Masonry Buildings", *J. Struct. Eng., ASCE*, **128**(7), 890-897.
- Milani, G., Lourenço, P. and Tralli, A. (2007), "3D homogenized limit analysis of masonry buildings under horizontal loads", *Eng. Struct.*, **29**(11), 3134-3148.
- Pallarés, F.J., Agüero, A. and Martín, M. (2006), "Seismic behaviour of industrial masonry chimneys", *Int. J. Solids Struct.*, **43**(7-8), 2076-2090.
- Prota, A., Marcarì, G., Fabbrocino, G., Manfredi, G. and Aldea, C. (2006), "Experimental in-plane behavior of tuff masonry strengthened with cementitious matrix-grid composites", *J. Compos. Constr., ASCE*, **10**(3), 223-233.
- Roca, P. (2006), "Assessment of masonry shear-walls by simple equilibrium models", *Constr. Build. Mater.*, **20**(4), 229-238.
- Shariq, M., Abbas, H., Irtaza, H. and Qamaruddin, M. (2008), "Influence of openings on seismic performance of masonry building walls", *Build. Environ.*, **43**(7), 1232-1240.
- Shrive, N.G. (2006), "The use of fibre reinforced polymers to improve seismic resistance of masonry", *Constr. Build. Mater.*, **20**(4), 269-277.
- Tasnimi, A.A. (2004), *Behavior of Brick Walls Recommended by Iranian Code of Practice for Seismic Resistant Design of Buildings*, Building and Housing Research Center, No. R-404, Tehran, Iran.
- Tasnimi, A.A. (2005), *Behavior of Confined and Non-confined Brick Buildings*, Natural Disaster Research Institute, Tehran, Iran.
- Turco, V., Secondin, S., Morbin, A., Valluzzi, M.R. and Modena, C. (2006), "Flexural and shear strengthening of un-reinforced masonry with FRP bars", *Compos. Sci. Technol.*, **66**(2), 289-296.
- Valluzzi, M.R., Tinazzi, D. and Modena, C. (2002), "Shear behavior of masonry panels strengthened by FRP laminates", *Constr. Build. Mater.*, **16**(7), 409-416.
- Yi, T., Moon, F.L., Leon, R.T. and Kahn, L.F. (2006), "Analyses of a Two-Story Unreinforced Masonry Building", *J. Struct. Eng., ASCE*, **132**(5), 653-662.